Theoretical treatment of channel mixing in excited Rb_2 and Cs_2 ultracold molecules: Determination of predissociation lifetimes with coordinate mapping

V. Kokoouline,[1,2] O. Dulieu,[1] R. Kosloff,[3] and F. Masnou-Seeuws[1]
[1]*Laboratoire Aimé Cotton, Bâtiment 505, Campus d'Orsay, 91405 Orsay Cedex, France*
[2]*The Institute of Physics, Saint Petersburg State University, Saint Petersburg 198904, Russia*
[3]*The Fritz Haber Research Center for Molecular Dynamics, The Hebrew University of Jerusalem, Jerusalem 91904, Israel*
(Received 7 February 2000; published 18 August 2000)

The treatment of the dynamics of ultracold molecules requires new theoretical tools. Previous work of the present authors [J. Chem. Phys. **110**, 9865 (1999)] for calculation of vibrational levels by a Fourier grid representation with use of adaptative coordinates is generalized here to the treatment of the bound-continuum interaction in a two-channel problem. Two numerical methods are presented: a time-dependent method using a Chebyshev propagator to compute the correlation function and a time-independent method with diagonalization of a Hamiltonian that includes an absorbing optical potential. In both cases the adaptative coordinate is defined by a numerical rather than an analytical procedure. Lifetimes are reported for the predissociated levels of the Rb_2 and Cs_2 0_u^+ $(ns+np^2P_{3/2})$ spectra, where $n=5,6$. The two numerical methods give similar results. The lifetimes increase with the vibrational quantum number proportionally to the classical vibration period estimated from the Le Roy–Bernstein law for an asymptotic R^{-3} potential, and the energy variation can be fitted to an analytical formula. The results are shown to be very sensitive to the molecular parameters, potentials, and couplings. The measured width of 8.5 GHz reported by Cline *et al.* [Phys. Rev. Lett. **73**, 632 (1994)] for one predissociated level of $^{87}Rb_2$ is reproduced. A strong isotopic effect is found for the rubidium dimer, the lifetimes of $^{85}Rb_2$ and $^{87}Rb_2$ levels differing by a factor of 3. Finally, we present a third approach, in the framework of a generalized two-channel quantum-defect theory, where lifetimes are determined by extrapolation of parameters fitted to Lu-Fano plots of computed bound levels below the $P_{1/2}$ dissociation limit. Excellent agreement is obtained with the numerical results, suggesting the possibility of fitting to experimental spectra.

PACS number(s): 33.80.Gj, 33.80.Ps, 31.15.−p, 31.50.+w

I. INTRODUCTION

The rapid development of photoassociation experiments [1,2] in a sample of cold alkali-metal atoms has supplied a wealth of information on the long-range excited molecules formed during the process. Besides their intrinsic interest for spectroscopic studies of asymptotic interactions, these short-lived molecules may decay by spontaneous emission into a bound molecular triplet or singlet ground state, as demonstrated already for Cs_2 [3], K_2 [4,5], and Rb_2 [6]. The photoassociation scheme therefore offers an interesting intermediate state for the production of ultracold molecules. In the near future, this scheme could even be efficient in transforming an atomic Bose-Einstein condensate into a molecular condensate [7–9]. Study of the dynamics of photoassociated molecules is thus a priority for theoreticians.

For that purpose, development of theoretical tools has proved necessary since, in the case of long-range R^{-3} potentials, the vibrational motion of the photoassociated molecule extends up to very large interatomic distances R where the local de Broglie wavelength becomes several orders of magnitude larger than at short range. Standard methods should be adapted to this novel situation, or alternatively new methods should be created. In a first paper [10], hereafter referred to as paper I, we have proposed a mapped Fourier grid representation of the Hamiltonian to determine energies and wave functions for vibrational levels close to the dissociation limit. The size of the grid in position and in momentum space, as well as the occupation of phase space, were efficiently optimized by use of an adaptative coordinate, mapped on the local de Broglie wavelength and defined through analytical or numerical transformation of the radial coordinate. Besides applications to vibrational motion in a single potential, generalization to a two-channel problem was considered, with the study of the strong perturbations in the Rb_2 $0_u^+(5s+5p\,^2P_{1/2,3/2})$ vibrational series. Then in a second paper [11], hereafter referred to as paper II, those calculations were further developed for Rb_2 and Cs_2, and their results analyzed to give a physical interpretation of the perturbations. For both heavy dimer molecules, although there exists strong spin-orbit coupling between the two Hund's case a $A\,^1\Sigma_u^+$ and b $^3\Pi_u$ potential curves, the picture of two Hund's case c $0_u^+(ns+np\,^2P_{1/2})$ and $0_u^+(ns+np\,^2P_{3/2})$ (where $n=5,6$ for Rb_2 and Cs_2, respectively) uncoupled adiabatic channels is never fully valid. Perturbations are present all over the spectral range (i.e., 5200 cm^{-1} in the case of Cs_2 and 5700 cm^{-1} in the case of Rb_2): the channel mixing is manifested through the oscillations of the binding energies and rotational constants between two limiting curves corresponding to the two unperturbed series for vibrational motion in the uncoupled adiabatic potentials. We showed that in the vicinity of the $(ns+np\,^2P_{1/2})$ dissociation limit, the spectra can be interpreted as one vibrational series perturbed by a quasicontinuum, and that it is possible to generalize quantum-defect concepts [12–14] in order to visualize the results on Lu-Fano plots.

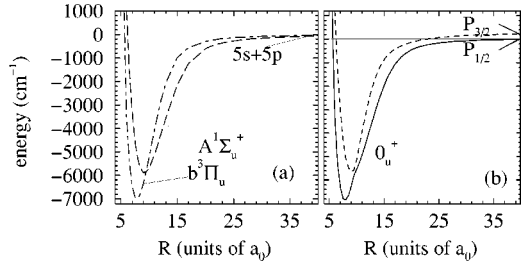

FIG. 1. Rb_2 potential curves without (a) and with (b) spin-orbit coupling. (a) Hund's case *a* $A\,^1\Sigma_u^+(5s+5p)$ (broken line) and $b\,^3\Pi_u(5s+5p)$ (dash-dotted line) curves from Ref. [16]; (b) Hund's case *c* $0_u^+(P_{1/2})$ and $0_u^+(P_{3/2})$ potential curves correlated, respectively, to the dissociation limits $(5s+5p\,^2P_{1/2})$ and $(5s+5p\,^2P_{3/2})$. A vibrational level close to the $P_{1/2}$ limit, and its turning point in the $0_u^+(P_{3/2})$ potential, are displayed for illustration.

The aim of the present work is to extend the methods of the two previous papers to the description of the bound-continuum interaction. Calculation of predissociation lifetimes are reported, taking as the main example the 0_u^+ spectra of Rb_2 in the energy range above the $5s+5p\,^2P_{1/2}$ and below the $5s+5p\,^2P_{3/2}$ dissociation limits (simply denoted $P_{1/2}$ and $P_{3/2}$ in the following), where the $P_{3/2}$ series of bound vibrational levels is perturbed by the continuum of the $P_{1/2}$ series. Results for the Cs_2 predissociated spectrum will also be presented. Generalization to the description of continuum-continuum interaction and interpretation of experimental data on fine-structure cross sections [15] will be treated in a forthcoming paper.

The potential curves and couplings are discussed in Sec. II. The two methods used for the numerical calculations, time-dependent with calculation of the correlation function and time-independent with absorbing potential, are explained in Sec. III. The results for the predissociation lifetimes are given in Sec. IV, where the sensitivity to molecular data is discussed in connection with experiment. In the final section, the computed lifetimes are compared with lifetimes extracted from quantum-defect theory (QDT) parameters fitted to the bound spectrum, showing how the problem of the uncertainty on short-range potentials could be bypassed.

Effects due to rotation or to hyperfine structure interaction will be neglected. Atomic units will be used except when otherwise stated, the unit for distances being 1 a.u.$=a_0=5.291\,77\times10^{-11}$ m. The energies of the levels will be given in cm^{-1}, the $P_{1/2}$ asymptote being considered as the origin, and the lifetimes will be given in picoseconds (ps).

II. THE TWO-CHANNEL PROBLEM: POTENTIALS AND COUPLINGS

In the calculations for Rb_2, we use Hund's case *a* potential curves $A\,^1\Sigma_u^+$ and $b\,^3\Pi_u$ from accurate quantum-chemistry calculations [16], matched at $R\approx17a_0$ to asymptotic calculations [17]. The corresponding curves, hereafter referred to as diabatic curves and labeled $V_A(R)$ and $V_B(R)$, respectively, are displayed in Fig. 1(a) for the Rb_2 dimer. For the Cs_2 dimer, the curves obtained by matching the *ab initio* curves of Meyer's group [18] to asymptotic

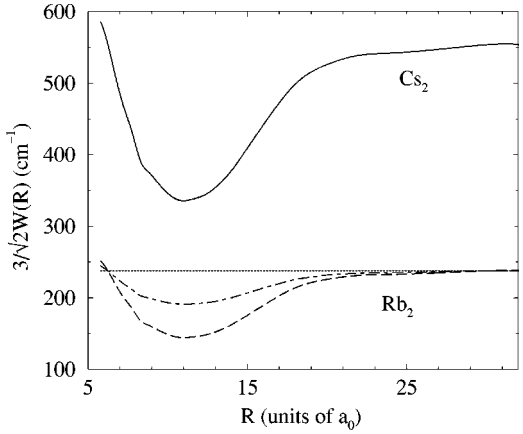

FIG. 2. Variation of the spin-orbit coupling used in the calculations as a function of internuclear distance *R*. The quantity represented is $(3/\sqrt{2})W(R)$, which is asymptotically equal to the atomic spin-orbit splitting $\Delta E_{SO}=554.1$ cm^{-1} for Cs_2 and $\Delta E_{SO}=237.6$ cm^{-1} for Rb_2. Solid line: *ab initio* calculations of Ref. [18] for Cs_2. Dashed line: $W^{m1}(R)$ for Rb_2, scaled on the preceding curve. Dot-dashed line: $W^{m2}(R)$ for Rb_2 (see text). Dotted line: constant spin-orbit coupling $W^{at}(R)$.

calculations [17] have been presented in paper II and will not be reproduced here. They are qualitatively similar to the Rb_2 curves, the crossing point being located at a slightly larger distance ($9.6a_0$ for Rb_2 and $10.4a_0$ for Cs_2). Introducing the spin-orbit coupling by an effective Hamiltonian and diagonalizing the 2×2 electronic Hamiltonian, as already described in paper II, yields the Hund's case *c* potential curves, displayed in Fig. 1(b). In the following, the two adiabatic potential curves $0_u^+(P_{1/2})$ and $0_u^+(P_{3/2})$ will be called $V_1(R)$ and $V_2(R)$, respectively.

The dynamical coupling between the two channels depends markedly upon the value of the nondiagonal spin-orbit coupling $W(R)$ in the vicinity of the crossing, at $R=R_c\approx10a_0$, of the $V_A(R)$ and $V_B(R)$ diabatic curves. At such distances, due to configuration mixing, $W(R)$ should be lower than the asymptotic atomic value $W^{at}=\Delta E_{SO}(\sqrt{2}/3)=0.471\Delta E_{SO}$, where ΔE_{SO} is the splitting between the $np\,^2P_{1/2}$ and $np\,^2P_{3/2}$ fine-structure levels. The curve $W(R)$ has been computed only for Cs_2 [18] (see Fig. 2) and $W(R_c)$ is indeed reduced by 35% as compared to W^{at}. For Rb_2 we have used two model curves $W^{m1}(R)$ and $W^{m2}(R)$ scaled on the computed Cs_2 curve and represented in Fig. 2. For $W^{m1}(R)$, the scaling factor is the ratio 237.6/554.1 of the atomic spin-orbit splittings, which gives at infinity the correct value $W^{at}=237.6$ cm^{-1} for a rubidium atom. In the crossing region, $W^{m1}(R_c)$ is then reduced by 35% relative to W^{at}. As the $4d$-$5p$ splitting for the rubidium atom is a factor of 2 larger than the $5d$-$6p$ splitting for the cesium atom, it is expected that due to a relatively weaker admixture of the $4d$ configuration, the reduction of the coupling might be smaller in the Rb_2 molecule: we have also considered the possibility for a 20% reduction, yielding the $W^{m2}(R)$ curve.

We have computed the eigenstates of the Hamiltonian **H** written as a 2×2 matrix in the diabatic representation,

$$\mathbf{H}=\mathbf{T}+\mathbf{V}, \tag{2.1}$$

TABLE I. Parameters used in the numerical calculations. For the time-dependent lifetime calculations, the absorbing zone starts at $R=80a_0$. For all calculations the grid starts at $5a_0$.

	Bound calculations				Time-ind. lifetimes calc.				Time-dep. lifetimes calc.			
Species	L	β	N_m	η	L	β	N_m	η	L	β	N_m	η
$^{85}Rb_2$	795	0.7	633	40	80	0.7	787	4.2	95	0.6	1024	4.2
$^{87}Rb_2$	795	0.7	639	40	80	0.7	797	4.2	95	0.61	1024	4.2
Cs_2	795	0.7	839	38	80	0.7	1279	2.6				

where **T** is the diagonal two-channel kinetic energy operator while **V** is written as

$$\mathbf{V(R)}=\begin{pmatrix} V_A(R) & W(R) \\ W(R) & V_B(R)-W(R)/\sqrt{2} \end{pmatrix}. \tag{2.2}$$

Adiabatic energies and wave functions are then deduced by rotation, the 2×2 transformation matrix M being obtained by diagonalization of **H**. A discussion of diabatic and adiabatic approaches for calculation of predissociation lifetimes has been given recently by Monnerville and Robbe [19] in the case of the CO molecule.

III. NUMERICAL CALCULATIONS OF THE LIFETIMES

A. Fourier grid representation and mapping procedure

We have used two approaches for the calculations: a time-dependent propagation with calculation of the correlation function and a time-independent method with an absorbing potential. Both approaches are based on a grid representation and take advantage of the mapping procedure.

The Fourier grid representation uses a basis set of plane waves e^{-ipR}. The coefficients of the expansion of a given wave function $\psi(R)$ are a set of values of this wave function in momentum space. On a grid of N points, the Hamiltonian **H** is represented by a $2N\times2N$ matrix, the matrix elements being given in paper I. The energies and wave functions of the bound levels are obtained by diagonalization of this matrix. The mapping procedure is expected to reduce the number of points N in the working grid. The mapped Fourier grid representation (MFGR) uses a basis set e^{-ipR} with R-dependent frequencies p scaled on the inverse of the local de Broglie wavelength $\lambda(R)$. In a two-adiabatic-channel problem, a lower limit for $\lambda(R)$ is estimated from the upper limit of the local classical kinetic energy $E^c_{\max}=V_1(\infty)+\Delta-V_1(R)$. In the present work, $V_1(\infty)=0$ is the energy of the $P_{1/2}$ asymptote while Δ has been chosen to be $\Delta E_{\rm SO}$, i.e., the difference between the $P_{3/2}$ and $P_{1/2}$ asymptotes. This is achieved by use of a working grid with a variable step $s_{\rm env}(R)$ defined as

$$s_{\rm env}(R)=\beta\frac{\pi}{\sqrt{2\mu[\Delta-V_1(R)+V_1(\infty)]}}. \tag{3.1}$$

The parameter $\beta<1$ is meant to increase the phase space in order to represent correctly the vanishing part of the wave functions in the classically forbidden region.

The originality of the present mapping procedure is the use of a numerical change of variable in Eq. (3.1) so that the real potential can be included. This choice minimizes the energy range of the Hamiltonian operator compared to an analytical mapping using, for instance, an asymptotic R^{-3} potential [10,20]. This has a direct consequence for time-dependent propagation methods which scale linearly with this energy range.

The efficiency of the mapping procedure is related to the reduction of the number of grid points. If the range of distances considered is $L=R_{\max}-R_{\min}$, the number of points on an equidistant grid will be

$$N_{\rm eq}=\frac{L}{\Delta R}=\frac{Lp_{\max}}{\pi}=\frac{L\sqrt{2\mu E_{\max}}}{\pi}, \tag{3.2}$$

where $E_{\max}$ is the maximum kinetic energy for a given potential. The number of points on the mapped grid can be calculated from (assuming $\beta=1$)

$$N_m=\int_L\frac{\sqrt{2\mu E(R)}dR}{\pi}, \tag{3.3}$$

where $E(R)$ is the local kinetic energy. Defining the ratio η between the two numbers,

$$\eta=\frac{N_{\rm eq}}{N_m}, \tag{3.4}$$

the efficiency of the MFGR calculations for bound states will be enhanced by a factor η^3 since the computing time for diagonalization scales as $O(N^3)$. For time-dependent calculations the enhancement factor is approximately $(\eta/2)\ln(\eta/2)$, since the bottleneck in the calculation is the FFT procedure. Table I summarizes the grid parameters and efficiency enhancement factors for the different calculations.

B. Time-propagation method for lifetime calculations

The principle of the method [21] relies upon direct determination of the lifetime of a given state from analysis of the correlation function

$$C(t)=\langle\psi_0|e^{-i\mathbf{H}t}|\psi_0\rangle=\langle\psi_0|\psi(t)\rangle, \tag{3.5}$$

which is the projection of the wave function $\psi(t)$ at a given time t on the initial wave function ψ_0, giving that part of the wave function of the initial state still ''surviving'' after the delay t. In case of an exponential decay of the population,

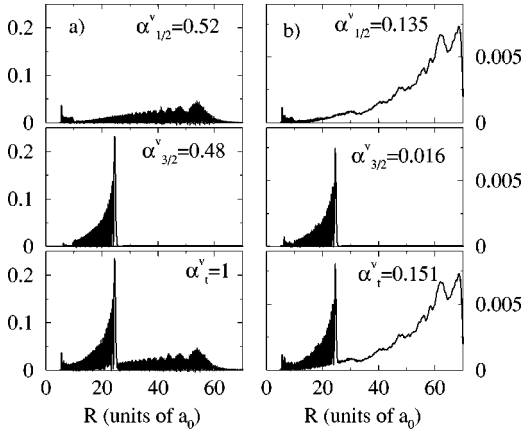

FIG. 3. (a) Adiabatic components of a two-channel predissociated vibrational wave function for $^{87}Rb_2$ (0_u^+) $(5s+5p^2P_{3/2})$, obtained by MFGR calculations at energy $E=25.37$ cm^{-1} above the $P_{1/2}$ dissociation limit. The upper panel shows $|\Psi^v_{1/2}(R)|^2$, which is the modulus of a continuum wave function represented here on a grid limited to a distance $R=80a_0$. The middle panel shows $|\Psi^v_{3/2}(R)|^2$, corresponding to bound motion in the potential $V_2(R)$. The lower panel shows the probability density as a function of internuclear distance for the total wave function. (b) Same as (a) after propagation during a time delay of 35 ps. The population in the $P_{3/2}$ channel is now decaying exponentially. The total population, α^v_t, on the two channels has been reduced from 1 to $\alpha^v_t=0.151$.

$$|\psi(t)|^2=e^{-t/\tau}|\psi_0|^2, \tag{3.6}$$

the lifetime τ is extracted from the correlation function as

$$\tau=-\frac{\ln|C(t_1)|-\ln|C(t_2)|}{2(t_1-t_2)}. \tag{3.7}$$

In the present work, we are considering a two-channel wave function in the mapped Fourier grid representation. As in paper II, for vibrational motion in the two coupled adiabatic potentials V_1 and V_2, corresponding, respectively, to the $P_{1/2}$ and $P_{3/2}$ dissociation limits, we write the two-channel wave function for a level v as

$$\Phi_v(t)=\Psi^v_{1/2}(R,t)|1\rangle+\Psi^v_{3/2}(R,t)|2\rangle. \tag{3.8}$$

In Eq. (3.8), $\Psi^v_{1/2}(R,t)$ and $\Psi^v_{3/2}(R,t)$ correspond to the nuclear wave functions for vibrational motion in channels 1 and 2, while $|1\rangle$ and $|2\rangle$ are the electronic states corresponding to the adiabatic potentials V_1 and V_2.

We define the relative population of the two channels through

$$\alpha^v_{3/2}(t)=1-\alpha^v_{1/2}(t)=\int|\Psi^v_{3/2}(R,t)|^2dR. \tag{3.9}$$

In order to define an initial function ψ_0 for the determination of the correlation function, we consider a wave function in the stationary MFGR computed as described in Sec. III A by diagonalization of the $2N\times2N$ Hamiltonian matrix. In contrast to bound level calculations, predissociated levels with an energy above the $P_{1/2}$ limit have a continuum component $\Psi^v_{1/2}(R)$. The computed energies and wave functions will therefore depend upon the size of the grid. As an illustration, we show in Fig. 3(a) the probability density for one predissociated wave function of Rb_2 computed by MFGR calculations for a grid described in Table I. One can see that the $\Psi^v_{3/2}$ component (middle panel) is looking like a typical bound level in a long-range R^{-3} potential, with a very strong probability density at the outer turning point. In contrast, the $\Psi^v_{1/2}$ component is qualitatively very different, being a continuum function. In order to save computer space, the grid step in Eq. (3.1) is computed choosing $\Delta=0$ and optimized for bound level calculation only, so that the continuum part of the total wave function is not well represented at large distances, which has no consequence for the results.

We then solve the time-dependent Schrödinger equation in order to determine the time-variation of the two-channel wave function $\Phi_v(t)$ with two components $\Psi^v_{1/2}(R,t)$ and $\Psi^v_{3/2}(R,t)$.

For the definition of the correlation function, it is possible to consider $\Phi_v(0)$ as the initial state ψ_0 or alternatively to extract the $\Psi^v_{3/2}(R,0)$ component and to propagate it in time.

(i) In the first case, the correlation function is the sum of two components:

$$\begin{aligned}C(t)&=C_{1/2}(t)+C_{3/2}(t)\\&=\int\Psi^v_{1/2}(R,t=0)\Psi^v_{1/2}(R,t)dR\\&\quad+\int\Psi^v_{3/2}(R,t=0)\Psi^v_{3/2}(R,t)dR.\end{aligned} \tag{3.10}$$

Whereas $\Psi^v_{3/2}(R,t)$ is decaying exponentially with time, the time decay of the continuum component is not exponential. The exponential behavior of $C(t)$ is reached only after the time delay necessary to filter out the $\Psi^v_{1/2}(R,t)$ component so that $C_{1/2}(t)$ becomes negligible.

(ii) In the second case, the component $C_{3/2}(t)$ is computed directly.

As the initial wave function is computed with a working grid different from the one used in the time-dependent calculation (see Table I), an interpolation procedure [10,22] has been implemented to transfer from one grid to the other. The propagation method consists of the expansion of the propagator $e^{-i\mathbf{H}t}$ in Chebyshev polynomials [22,23]. The order of the polynomial to be used depends on the energy range of the Hamiltonian matrix representation. The use of the present mapping procedure, where the change of coordinate is defined numerically with the real potential $V_1(R)$ instead of an analytical formula that uses the asymptotic R^{-3} potential, is efficient since it minimizes the energy range. In order to avoid reflection at the end of the grid, the outgoing flux is smoothly absorbed by an absorbing potential, starting at a distance of $80a_0$, as described below.

We have represented in Fig. 3(b) the wave functions obtained by propagating, for a time of 35 ps, the two-component wave function represented in Fig. 3(a) at time $t=0$. The total norm $\alpha_v(t)$ of the wave function represented

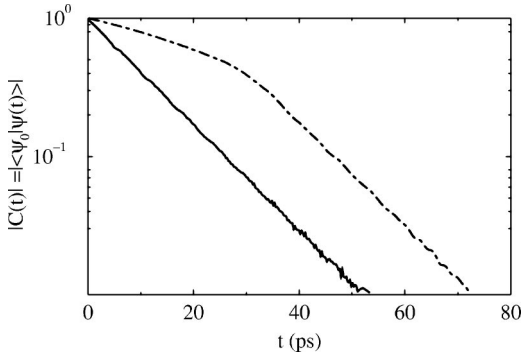

FIG. 4. The correlation functions $C(t)$ (dotted line) and $C_2(t)$ (solid line) for a predissociated level of $^{87}Rb_2(0_u^+)(5s+5p\,^2P_{3/2})$, at energy $E=25.37$ cm^{-1} above the $P_{1/2}$ asymptote. After a time delay ($t_0\approx 30$ ps) the slope of the two curves becomes identical due to the disappearance of the $P_{1/2}$ component present in the initial wave function.

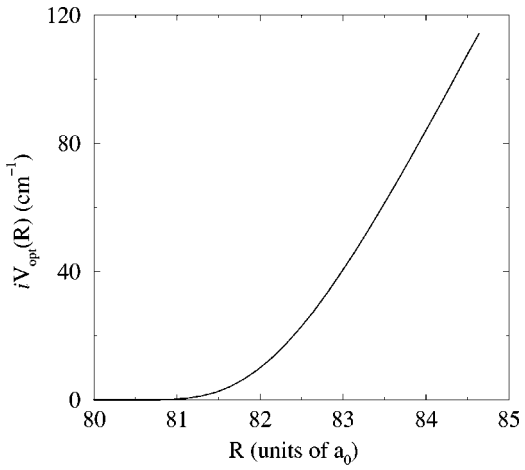

FIG. 5. The optical potential used for calculations of lifetimes as defined in Eq. (3.11) in text, with parameters $A_5=0.000\,29$, $N_{\rm opt}=13.22$, $L_{\rm opt}=4.8a_0$, $R_0=80a_0$.

on the grid is no longer 1, but 0.151: indeed, 85% of the probability has now escaped, the wave packet in channel 1 having reached distances larger than the grid length $L=80a_0$. Figure 4 gives examples of the correlation functions $C(t)$ and $C_{3/2}(t)$ for the same predissociated level. While the second one clearly has an exponentially decreasing behavior, the first one corresponds to two characteristic times, a short one for the elimination of the $P_{1/2}$ component, and a long one which is the lifetime of the $P_{3/2}$ component. Therefore, in logarithmic scale the two curves become parallel for $t\approx 30$ ps. The propagation during the time $t\in(0\text{ ps},30\text{ ps})$ is thus working as a time filter for the predissociated wave function [21] selecting from the initial wave function only that part belonging to the bound spectrum. For $t>30$ ps, the population of the predissociated state is decaying exponentially, with the same time constant as $\alpha^v_{3/2}$. Small oscillations appear in the two curves of Fig. 4 when time is increasing. They are relatively small in amplitude, as the figure is drawn in logarithmic scale, and can be interpreted as a beating phenomenon, due to coupling via the continuum between the resonance at $E_v^{\rm res}=25.37$ cm^{-1} and a neighboring one.

C. The mapped FGR method with an absorbing potential for lifetime calculations

As a second tool for the calculation of lifetimes and as a test for the previous results, we also solved the stationary Schrödinger equation (using MFGR) with an absorbing (optical) potential at the end of the grid. The Hamiltonian now has both real and imaginary components: diagonalization of its matrix in the mapped Fourier grid representation then yields complex eigenvalues $E_v^{\rm res}+i\Gamma_v/2$, where $E_v^{\rm res}$ is the energy and Γ_v is the width of the vibrational level v.

The potential $V_{\rm opt}$ should be zero in the region where the molecular potentials are not negligible, and purely imaginary in the asymptotic region, where the two atoms no longer interact. The best possible choices were discussed by Vibók *et al.* [24] and Monnerville *et al.* [19] and we use one of the potentials proposed in Ref. [24],

$$V_{\rm opt}=-iA_5\left[N_{\rm opt}\exp\left(-\frac{2L_{\rm opt}}{R-R_0}\right)\right], \tag{3.11}$$

with parameters A_5, $N_{\rm opt}$, and $L_{\rm opt}$ calculated according to the quoted reference. For Rb_2: $A_5=0.000\,29$ a.u., $N_{\rm opt}=13.22$, $L_{\rm opt}=4.8a_0$; and for Cs_2: $A_5=0.000\,355$ a.u., $N_{\rm opt}=13.22$ a.u., $L_{\rm opt}=2.5a_0$. R_0 is the starting point of the optical potential and was chosen as $80a_0$. (See Fig. 5.) This potential should be added to the physical potential V_1 on the $P_{1/2}$ channel in order to absorb the outgoing flux. However, the bound vibrational wave functions in the V_2 potential were shown to remain unchanged when the optical potential was added to V_2. Therefore, in calculations performed in the diabatic representation, we considered the potentials $V_A+V_{\rm opt}$ and $V_B+V_{\rm opt}$ in the matrix of Eq. (2.2).

The precision of the method was controlled in different ways.

(i) First, we verified the stability of results with respect to a change of the parameters of the absorbing potential. Moving the starting point R_0 from $80a_0$ to $160a_0$ resulted in a 5×10^{-5} relative change in the calculated lifetimes. In the Rb_2 case, increasing the length $L_{\rm opt}$ of the absorbing region from $4.8a_0$ to $20a_0$ modifies the lifetimes by less than 0.01%. Finally, a modification of the strength A_5 of the absorbing potential was introduced under the conditions defined by Ref. [24] to ensure that the outgoing flux is not reflected from the absorbing potential: such modification did not affect the calculated lifetimes.

(ii) Second, we compared with the time-dependent method as discussed below in Sec. III D.

D. Comparison of the two methods

In the case of $^{85}Rb_2$, the lifetimes computed as described above, with the choice $W(R)=W^{\rm at}$ for the coupling, are displayed in Fig. 6 as a function of the level energy $E_v^{\rm res}$, taking the $P_{1/2}$ dissociation limit as the energy origin. For the lower levels $E_v\leqslant 100$ cm^{-1}, the lifetimes are small and the two methods yield results that are almost identical. When the

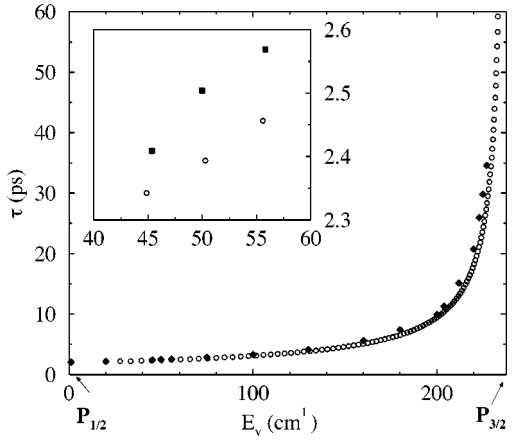

FIG. 6. Lifetimes for the predissociated levels of $^{85}Rb_2$ (0_u^+) $(5s+5p\,^2P_{3/2})$ as a function of the energy above the $P_{1/2}$ asymptote: comparison of the results from the time-dependent method (diamonds) and the time-independent method (circles). For the sake of clarity, as the results are very close, only some levels are presented for the time-dependent calculations. The inset shows details of the comparison in the 40–60 cm^{-1} energy range.

level energy is increasing, the lifetimes also increase and for relatively large values ($\tau > 20$ ps) there is a divergence of a few % between the results obtained by two methods, the results of the time-dependent method being systematically larger. This discrepancy may be attributed to some uncertainty in the determination of the slope of the $C(t)$ curve:

$$d\tau = \left(\frac{t \Delta \ln C}{2(\ln C)^2} \right) = \tau \frac{\Delta \ln C}{\ln C} = 2(\Delta \ln C) \frac{\tau^2}{t}, \quad (3.12)$$

where $\Delta \ln C$ is the uncertainty in the determination of the slope of the correlation function. The relative error is

$$\frac{d\tau}{\tau} = 2(\Delta \ln C) \frac{\tau}{t}. \quad (3.13)$$

Thus, for a fixed propagation time the relative error in the determination of τ is larger for levels with a longer lifetime. In order to obtain the same accuracy, the wave functions of levels with large τ should be propagated for a longer time.

In general, in calculating resonance eigenvalues the real part of the eigenvalue, the energy, converges much faster than the lifetime [25]. The convergence rate of lifetimes for the time-dependent method is $O(1/t)$. For the time-independent diagonalization method the convergence depends on the properties of the optical potential. The lifetimes were checked to be stationary with respect to variation in the parameters of the optical potential indicating an exponential convergence. Hybrid methods which are a combination of direct propagation and diagonalization known as filter diagonalization seem to be the best suited for most problems [25,26]. However, we may conclude here that for the particular case of cold atoms the direct diagonalization methods seem to be both more accurate and more convenient.

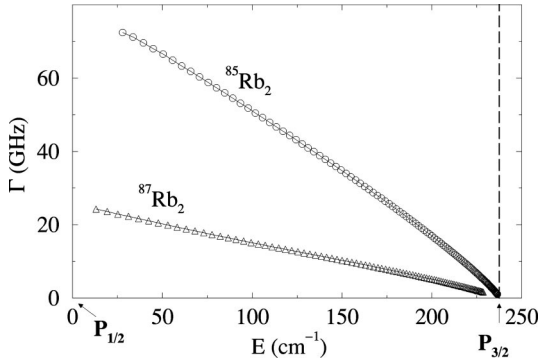

FIG. 7. Predissociation widths $\Gamma_v = 1/\tau_v$ computed for two isotopes, $^{85}Rb_2$ (circles) and $^{87}Rb_2$ (triangles), as a function of the level energy above the $P_{1/2}$ asymptote. The lines represent a fit, according to Eq. (4.3) in text. The widths are proportional to the classical frequency of the vibrational motion.

IV. LIFETIMES OF PREDISSOCIATED LEVELS

We have computed the energies E_v^{res} (hereafter given relative to the $P_{1/2}$ asymptote) and lifetimes $\tau_v = 1/\Gamma_v$ for the predissociated vibrational levels in the 0_u^+ spectrum of the two isotopes $^{85}Rb_2$ and $^{87}Rb_2$, as well as for $^{237}Cs_2$, considering both constant coupling W^{at} and R-dependent coupling. The first important result is the strong isotopic effect observed in the lifetimes, which are smaller by a factor of 3 in the case of $^{85}Rb_2$, as can be seen in Fig. 7.

The strong increase of the lifetime near the $P_{3/2}$ asymptote can be qualitatively explained by an increase of the period of the classical oscillations at higher energy. Half the classical period for the motion in a potential $U(R) = D - (C_3/R^3)$ at energy E_v^{res} is given by

$$\frac{T}{2} = \sqrt{\frac{\mu}{2}} \int_{R_{min}}^{R_{max}(E_v)} \frac{dR}{\sqrt{E_v - U(R)}}$$

$$\approx \frac{1}{3} \sqrt{\frac{\mu\pi}{2}} C_3^{1/3} \frac{\Gamma(\frac{5}{6})}{\Gamma(\frac{4}{3})} (D - E_v^{res})^{-5/6}, \quad (4.1)$$

where the integral is calculated as in Ref. [27] assuming that the contribution of the asymptotic region is dominating. In Eq. (4.1), D is the energy of the dissociation limit equal to the splitting between the $P_{1/2}$ and $P_{3/2}$ asymptotes, $D = \Delta E_{SO}$. Assuming that the coupling between the two potentials is effective only at relatively short distances, where the motion can be considered as independent of the energy of the level, we can expect an analytical energy dependence of the lifetimes,

$$\tau(E_v^{res}) = \alpha (D - E_v^{res})^{-5/6}, \quad (4.2)$$

where the parameter α depends upon the physical parameters (transition probability and time delay) in the short-range region and is proportional to $\sqrt{\mu}$. This interpretation will be developed in further work.

The predissociation width should then decrease to the value 0 at the asymptote varying as

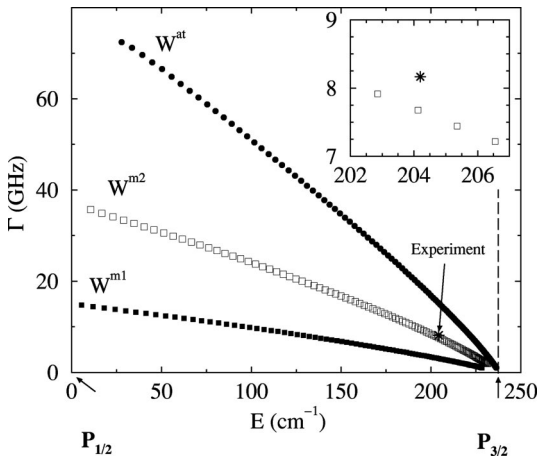

FIG. 8. Predissociation widths for the vibrational levels of $^{85}Rb_2\ 0_u^+\ (5s+5p\ ^2P_{3/2})$ computed for three choices of the molecular spin-orbit coupling $W(R)$ (see Fig. 2) between the $b\ ^3\Pi_u$ and $A\ ^1\Sigma_u$ diabatic potential curves: W^{at} (dark circles), W^{m1} (white squares), and W^{m2} (dark squares). The experimental value from [28] (corresponding to a lifetime $\tau \approx 20$ ps) is represented by a big star. The inset shows details of the results in this energy region.

$$\Gamma = \frac{(D - E_v^{\mathrm{res}})^{5/6}}{\alpha}. \tag{4.3}$$

It can be verified in Fig. 7 that the variation of the computed widths as a function of the level energy is indeed well fitted by an analytical curve (4.3) with parameters $\alpha = 189.5$ ps $(\mathrm{cm}^{-1})^{5/6}$ for $^{85}Rb_2$ and $\alpha = 628.3$ ps $(\mathrm{cm}^{-1})^{5/6}$ for $^{87}Rb_2$. Thus, for all predissociated levels, the lifetime decreases by a factor of 3 when the reduced mass decreases by less than 3% (from $\mu = 79\,212.88$ a.u. to $\mu = 77\,392.38$ a.u.). The classical period decreases only by 0.5%. This means that due to a phase effect the short-range transition probability from one channel to the other is very sensitive to the reduced mass. In order to get more insight into this strong isotopic effect, we have calculated lifetimes for fictitious isotopes of Rb_2 with a reduced mass differing from that of the two physical isotopes. For example, the lifetime increases by one order of magnitude ($\alpha = 6366$) when the reduced mass is decreased down to $\mu = 75\,000$ a.u. However, for an ever smaller reduced mass, $\mu = 70\,000$, the calculations yield $\alpha = 455$, so that the lifetime is even shorter than for $^{87}Rb_2$. As in paper II, we can link this behavior to a phase effect, where, for highly excited levels with high vibrational number, the phases are very large compared to π so that a small relative change becomes non-negligible when considering the phase modulo π.

The large difference in lifetimes for the two isotopes of Rb_2 is likely to explain the difference of a factor of about 3 in the trap loss signal observed by Wallace *et al.* [15] for $^{85}Rb_2$ and $^{87}Rb_2$. It was interpreted in the quoted reference as a possible consequence of the difference of the hyperfine structure splitting. The present results suggest that it could also be explained as due to a difference in coupling effect, due to a phase variation when the mass is modified.

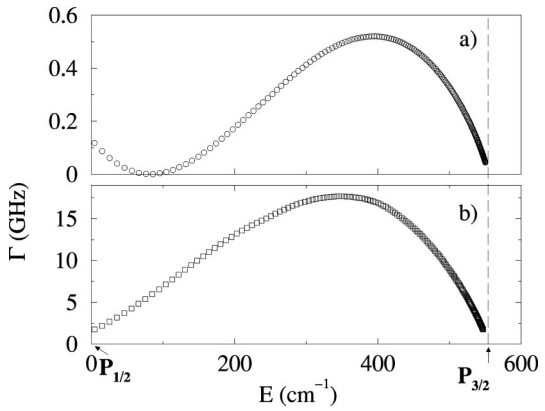

FIG. 9. Predissociation widths for the levels of $Cs_2\ 0_u^+\ (6s+6p\ ^2P_{3/2})$ as a function of the energy above the $P_{1/2}$ asymptote, computed for two choices of the spin-orbit coupling $W(R)$ between the diabatic $b\ ^3\Pi_u$ and $A\ ^1\Sigma_u$ curves. (a) $W(R)$ is constant and equal to $W^{at} = (\sqrt{2}/3) \times 554.1\ \mathrm{cm}^{-1}$. (b) $W(R)$ is R-dependent and varying as displayed at the top of Fig. 2.

As in paper I, we find that the channel mixing, and hence the isotopic effect, is highly sensitive to molecular data. This is demonstrated in Fig. 8, where the width for the levels in the $P_{3/2}$ series for $^{85}Rb_2$ is shown to be reduced by a factor of 4 when a variable spin-orbit coupling $W^{m1}(R)$ scaled on the cesium curve is introduced. Excellent agreement with the experimental width of Ref. [28] is obtained when $W^{m2}(R)$ is chosen for the spin-orbit coupling. However, this choice is fully arbitrary, as a slight modification in the potential curves would lead to another optimal value for the coupling factor. We shall therefore discuss in the following section how lifetimes can be extracted from parameters fitted to the bound spectra, taking advantage of the accuracy of spectroscopic information and of the asymptotic character of the potentials during most of the period of the vibrational motion.

The results for Cs_2 are displayed in Fig. 9. One should note the reduction of the widths by more than one order of magnitude when turning from Rb_2 to this heavier molecule with larger spin-orbit splitting, for which the picture of unperturbed motion in the single V_2 adiabatic potential is more valid. We find an important difference in the lifetimes computed with constant and variable spin-orbit coupling: the adiabatic character of the problem is reduced when the molecular spin-orbit coupling is considered, yielding larger widths or smaller lifetimes. The asymptotic analytical model of Eqs. (4.2) and (4.3) for the energy variation of the lifetimes and widths is valid only for the most excited levels, in a 100 cm^{-1} energy range below the dissociation limit. For lower levels, the time spent in the inner region and the transition probability can no longer be considered as energy-independent.

V. ASYMPTOTIC METHOD FOR ESTIMATION OF THE LIFETIMES FROM PARAMETERS FITTED ON BOUND SPECTRUM

In paper II, we have proposed an interpretation of the perturbations in the vibrational series below the $P_{1/2}$ limit in

the framework of a two-channel generalized quantum-defect theory. First, we have checked that due to the asymptotic R^{-3} character of both the adiabatic potentials $V_1(R)$ and $V_2(R)$, calculations neglecting the coupling term will yield two series of bound vibrational levels v_1 and v_2 verifying a Le Roy–Bernstein law [27] close to the dissociation limit,

$$E(v_i)=D_i-[H_3^i(v_D^i-v_i)]^6. \tag{5.1}$$

This law is relating the energy of a given vibrational level to its quantum number v_i by use of two constants where D is the energy of the dissociation limit while H_3 is linked to the reduced mass μ and to the asymptotic potential $-C_3/R^3$ through $H_3=0.991\,485/[\mu^{1/2}(C_3)^{1/3}]$. The law does not depend upon the absolute numbering, and an effective quantum number $n_i^*=v_D^i-v_i$ or a quantum defect μ_i can easily be related to the quantity $(v_D^i-v_i)$, which by definition is zero at the dissociation limit. Generalization to a wider energy range could be performed by means of a numerical law relating the energy of the level to the effective quantum number. Once the coupling between the two channels is introduced, we have shown that for a wide ($\approx$1000 cm^{-1}) energy range, the computed vibrational energies can be fitted by three parameters equivalent to two generalized quantum defects and one coupling parameter. This requires generalization of the Lu-Fano law,

$$\tan[\pi(-n_1^*+\mu_1)]=\frac{R_{1,2}^2}{\tan[\pi(-n_2^*+\mu_2)]}. \tag{5.2}$$

As such parameters have a very weak dependence upon the energy, it is valuable, in the spirit of quantum-defect theory [14], to extrapolate them above the $P_{1/2}$ dissociation limit in order to extract predissociation lifetimes from the formula

$$\tau^{-1}=\Gamma(v_2)=\frac{2}{\pi}R_{1,2}^2(E_{v_2+1}-E_{v_2}). \tag{5.3}$$

In Eq. (5.3), v_2 is the vibrational numbering of a level of the $P_{3/2}$ series. Once the coupling is introduced, this level has a new effective quantum number so that it is shifted by the quantity

$$\delta E(v_2)=\mu_2(E_{v_2+1}-E_{v_2}). \tag{5.4}$$

We give in the following a comparison of lifetimes computed by the various methods for $^{87}Rb_2$. For one predissociated level just above the $P_{1/2}$ limit, the energy and the width calculated directly are $E_v^{\rm res}=13.037$ cm^{-1} and $\Gamma_v=24.2$ GHz. Using the two parameters $R_{1,2}=0.47$ and $\mu_2=-0.36$ derived from the bound spectrum, the asymptotic formula above predicts for the levels $E_{v2}^{\rm res}=13.052$ cm^{-1} and $\Gamma_{v2}=26.4$ GHz. For a level situated far from the region of determination of parameters $R_{1,2}$ and μ_2, the direct calculations give $E_v^{\rm res}=201.216$ cm^{-1} and $\Gamma_v=4.97$ GHz. The prediction with the same parameters $R_{1,2}$ and μ_2 give $E_{v2}^{\rm res}=201.208$ cm^{-1} and $\Gamma_{v2}=5.62$ GHz.

TABLE II. Comparison of the generalized quantum defects μ_1, μ_2, and coupling parameter $R_{1,2}$ extracted from various calculations in the case of $^{85}Rb_2$. The first column represents a fit to the quasiresonances present in the $P_{3/2}$ bound spectrum below the $P_{1/2}$ dissociation limit.

	Relative population	Lu-Fano plot	Lifetime calculation
μ_1	not defined	0.82	not defined
μ_2	0.19	0.185	0.18
$R_{1,2}$	0.76	0.74	0.80

Alternatively, from the computed lifetimes and vibrational energy splitting, an interaction parameter can be obtained from

$$R_{1,2}=\frac{\pi}{2\tau(E_{v+1}^{\rm res}-E_{v2}^{\rm res})}, \tag{5.5}$$

while a quantum defect can be estimated from the level shift by inverting Eq. (5.4),

$$\mu_2(v_2)=\frac{\delta E(v^{\rm res})}{(E_{v+1}^{\rm res}-E_v^{\rm res})}. \tag{5.6}$$

We have verified that in the case of $^{85}Rb_2$ there are $\approx$200 predissociated levels above the $P_{3/2}$ limit for which μ_2 is nearly constant, varying by less than 0.1, while the coupling parameter varies by a few percent.

The parameters μ_2 and $R_{1,2}$ can also be extracted from the relative population $\alpha_{3/2}^v$ of the $\Psi_{3/2}^v(R)$ component for *bound* levels just below the $P_{1/2}$ dissociation limit [11]. In this region the total bound spectrum can be considered as a set of quasiresonances of the V_2 state ''predissociated'' in the quasicontinuum created by the high density of $P_{1/2}$ vibrational levels.

The results are reported in Table II, where the parameters μ_1, μ_2, and $R_{1,2}$ are extracted from three different sources: the relative population of the $P_{3/2}$ component, the Lu-Fano plot, and the lifetime calculations (time-independent and time-dependent). For the energy domain between the two dissociation limits, the relative accuracy of the prediction of the widths and positions of resonances of Rb_2 using the Lu-Fano plot is estimated as 10^{-4} for positions and 10% for widths.

TABLE III. Comparison of generalized Lu-Fano parameters μ_1, μ_2, $R_{1,2}$ for different species and different choices of molecular spin-orbit coupling W.

	μ_1	μ_2	$R_{1,2}$
$^{85}Rb_2$, $W^{\rm at}$	0.82	−0.81	0.74
$^{85}Rb_2$, W^{m1}	0.77	−0.76	0.47
$^{85}Rb_2$, W^{m2}	0.67	−0.66	0.62
$^{87}Rb_2$, $W^{\rm at}$	0.37	−0.36	0.47
Cs_2, $W^{\rm at}$	0.048	−0.046	0.03
Cs_2, W^m	0.097	−0.096	0.1

Positions of *perturbed bound levels* below $P_{1/2}$ limit can be predicted using three Lu-Fano parameters down to -1000 cm^{-1} with accuracy varying from 10^{-5} for $E=-200$ cm^{-1} to 5×10^{-4} for $E=-1000$ cm^{-1}.

The Lu-Fano representation therefore yields a very compact way of representing both bound and predissociated spectrum. We give in Table III the values of the parameters that we obtain from calculations with the present set of potentials and various choices for the coupling, showing the huge sensitivity to the choice of molecular data. We should note in particular the very small value of the coupling parameter R_{12} for Cs_2 when constant spin-orbit coupling is considered and the picture of two uncoupled Hund's case *c* channels is nearly valid. We should also note the spectacular variation of the same parameter in the Rb_2 case, when either the coupling or the reduced mass are changed. This confirms the necessity of fitting parameters directly to the photoassociation spectra once they are available.

If a part of the discrete spectrum close to the dissociation limit is known (for example, from a photoassociation spectroscopy experiment), the widths and positions of predissociated resonances can be predicted. The asymptotic shift $\delta(v_2)$ of the continuum wave function of the resonances can be defined also from the parameter μ_1 by

$$\delta(v_2)=\pi\mu_1. \tag{5.7}$$

VI. CONCLUSION AND PERSPECTIVES

In the present paper we have presented calculations of the predissociation lifetimes for vibrational levels of an excited ultracold molecule, when the vibrational motion extends out to large distances in a potential with asymptotic R^{-3} behavior. Application to predissociation effects in the 0_u^+ spectrum of Rb_2 and Cs_2 between the $ns+np\,^2P_{1/2}$ and $^2P_{3/2}$ dissociation limits has been reported, in the framework of two-coupled-channel calculations.

Two numerical grid methods making use of a Fourier grid representation have been described: a mapped time-dependent method using a Chebyshev propagator to compute the correlation function and a mapped time-independent method with diagonalization of a Hamiltonian including an absorbing optical potential. The mapping procedure introduced in previous work [10] for bound level calculations has been generalized to problems involving a continuum. The size of the calculations is reduced by adapting the grid step to the variation of the local de Broglie wavelength through definition of a new radial coordinate. The originality of the mapping procedure lies in the definition of this adaptative coordinate through a numerical formula making use of the real potential $V_1(R)$ rather than an analytical formula for an asymptotic R^{-3} potential [20]. For time-dependent propagation we have shown that this procedure is efficient since it minimizes the energy range. The predissociation lifetimes computed by the two numerical methods agree within a few percent. The time-independent method with an optical potential is both more accurate and more convenient. This conclusion may seem paradoxical, as the scaling of the computation effort with the number N of grid points is N^3 for diagonalization and only $N\ln N$ for time propagation. However, the mapping reduces N such that it makes the diagonalization feasible and the method more efficient.

The computed lifetimes for the bound levels in the $0_u^+(^2P_{3/2})$ potential predissociated by the $0_u^+(^2P_{1/2})$ continuum are found to be increasing as a function of the energy E above the $^2P_{1/2}$ limit, being proportional to the classical vibrational period. In accordance with the Le Roy–Bernstein model [27], the latter varies asymptotically as $(D-E)^{-5/6}$, where D is the dissociation limit. We have shown that the computed predissociation lifetimes can be fitted by such a law in the entire energy range for Rb_2 but only in a 100 cm^{-1} energy range for Cs_2. This can be understood within a simple model where the coupling beween the two channels is limited to the short-range region where the motion is energy independent. As for bound state calculations, the results depend markedly upon the choice of potentials and coupling, and we have discussed the effect of the R dependence of the spin-orbit coupling. With a reasonable choice, it is possible to reproduce the only published experimental value of 19 ps measured for a level of $^{87}Rb_2$ [28]. For all levels, a strong isotopic effect is found in the lifetimes, which for one choice of the coupling are found to be three times larger for $^{87}Rb_2$ than for $^{85}Rb_2$. This effect could be the correct interpretation for the isotopic difference in the fine-structure changing cross sections observed experimentally [15] in 1992 and then attributed to the isotopic variation of the hyperfine structure.

The numerical methods presented in the present paper provide results with spectroscopic accuracy once the potentials and couplings are known. However, for heavy dimers such as Rb_2 and Cs_2, the most accurate *ab initio* calculations determine short-range potential curves with an uncertainty of a few cm^{-1}: only the asymptotic part of the curves can be known with the required accuracy. Nevertheless, for the levels that we are studying, the vibrational motion is governed by the asymptotic region, and this is the reason why the numerical results could be fitted by a formula corresponding to Le Roy–Bernstein model. The effect of the ill-known short-range region may be represented by energy-independent parameters, and this should allow us to bypass the uncertainty on potentials at small distances. In order to check this point, we have used a generalized quantum-defect theory and Lu-Fano plots to extract parameters from the bound spectrum and extrapolate them through the dissociation limit. For a given set of potentials and couplings, the lifetimes calculated by this asymptotic procedure are in excellent agreement with the results of numerical calculations.

We may therefore conclude that once experimental photoassociation spectra are available, the spectroscopic accuracy of the energies of bound levels below the $P_{1/2}$ asymptote can be exploited to determine the relevant parameters, and we extrapolate them above the first dissociation threshold to deduce accurate lifetimes. Possible further extrapolation above the $P_{3/2}$ threshold should also be considered in future work as a way to compute accurate fine-structure transition cross sections relevant to trap loss experiments [15].

[1] H.R. Thorsheim, J. Weiner, and P.S. Julienne, Phys. Rev. Lett. **58**, 2420 (1987).
[2] P.D. Lett, K. Helmerson, W.D. Philips, L.P. Ratliff, S.L. Rolston, and M.E. Wagshul, Phys. Rev. Lett. **71**, 2200 (1993).
[3] A. Fioretti, D. Comparat, A. Crubellier, O. Dulieu, F. Masnou-Seeuws, and P. Pillet, Phys. Rev. Lett. **80**, 4402 (1998).
[4] N. Nikolov, E.E. Eyler, X.T. Wang, J. Li, H. Wang, W.C. Stwalley, and Ph. Gould, Phys. Rev. Lett. **82**, 703 (1999).
[5] N. Nikolov, J.R. Enscher, E.E. Eyler, H. Wang, W.C. Stwalley, and Ph. Gould, Phys. Rev. Lett. **84**, 246 (2000).
[6] C. Gabbanini, A. Fioretti, A. Lucchesini, S. Gozzini, and M. Mazzoni, Phys. Rev. Lett. **84**, 2814 (2000).
[7] P.S. Julienne, K. Burnett, Y.B. Band, and W.C. Stwalley, Phys. Rev. A **58**, R797 (1998).
[8] M. Mackie and J. Javanainen, Phys. Rev. A **60**, 3174 (1999).
[9] E. Timmermans, P. Tommasini, M. Hussein, and A. Kerman, Phys. Rep. **315**, 199 (1999).
[10] V. Kokoouline, O. Dulieu, R. Kosloff, and F. Masnou-Seeuws, J. Chem. Phys. **110**, 9865 (1999).
[11] V. Kokoouline, O. Dulieu, and F. Masnou-Seeuws, Phys. Rev. A **62**, 022504 (2000).
[12] K.T. Lu and U. Fano, Phys. Rev. A **2**, 81 (1970).
[13] M.J. Seaton, Rep. Prog. Phys. **46**, 167 (1994).
[14] H. Friedrich, *Theoretical Atomic Physics* (Springer, New York, 1998).
[15] C.D. Wallace, T.P. Dinneen, K.Y.N. Tan, T.T. Grove, and P.L. Gould, Phys. Rev. Lett. **69**, 897 (1992).
[16] M. Foucrault, Ph. Millié, and J.P. Daudey, J. Chem. Phys. **96**, 1257 (1992).
[17] M. Marinescu and A. Dalgarno, Phys. Rev. A **52**, 311 (1995).
[18] N. Spies, Ph.D. thesis, Fachbereich Chemie, Universität Kaiserslautern (1989).
[19] M. Monnerville and J.M. Robbe, Eur. Phys. J. D **5**, 381 (1999).
[20] E. Tiesinga, C.J. Williams, and P.S. Julienne, Phys. Rev. A **57**, 4257 (1998).
[21] O. Dulieu, R. Kosloff, F. Masnou-Seeuws, and G. Pichler, J. Chem. Phys. **107**, 10 633 (1997).
[22] R. Kosloff, Annu. Rev. Phys. Chem. **45**, 145 (1994).
[23] H. Tal Ezer and R. Kosloff, J. Chem. Phys. **81**, 3967 (1984).
[24] Á. Vibók and G.C. Balint-Kurti, J. Phys. Chem. **96**, 8712 (1992).
[25] S. Skokov, J.M. Bowman, and V.A. Mandelshtam, PCCP Phys. Chemistry Chem. Phys. **1**, 1279 (1999).
[26] M.R. Wall and D. Neuhauser, J. Chem. Phys. **102**, 8011 (1995).
[27] R.J. LeRoy and R.B. Bernstein, J. Chem. Phys. **52**, 3869 (1970).
[28] R.A. Cline, J.D. Miller, and D.J. Heinzen, Phys. Rev. Lett. **73**, 632 (1994).